

# Spectral element modelling and analysis of a pipeline conveying internal unsteady fluid

U. Lee\*, J. Park

*Department of Mechanical Engineering, Inha University, 253 Yonghyun-Dong, Nam-Ku, Incheon 402-751, Republic of Korea*

Received 26 January 2005; accepted 17 September 2005

Available online 21 October 2005

---

## Abstract

In this paper, a spectral element model is developed for the uniform straight pipelines conveying internal unsteady fluid. Four coupled pipe-dynamics equations are derived first by using the Hamilton's principle and the principles of fluid mechanics. The transverse displacement, the axial displacement, the fluid pressure and the fluid velocity are all considered as the dependent variables. The coupled pipe-dynamics equations are then linearized about the steady-state values of the fluid pressure and velocity. As the final step, the spectral element model represented by the exact dynamic stiffness matrix, which is often called spectral element matrix, is formulated by using the frequency-domain solutions of the linearized pipe-dynamics equations. The fast Fourier transform (FFT)-based spectral dynamic analyses are conducted to evaluate the accuracy of the present spectral element model and also to investigate the structural dynamic characteristics and the internal fluid transients of an example pipeline system.

© 2005 Elsevier Ltd. All rights reserved.

*Keywords:* Pipe-dynamics; Internal unsteady flow; Spectral element method

---

## 1. Introduction

The pipelines in chemical plants, pipeline arrays in steam generators, oil pipelines, pump discharges, propellant fluid lines of liquid-filled rockets, and human circulation are typical examples which are used for the transport of high velocity pressured fluids. The time-varying conditions imposed by pump or valve operations may change the internal fluid field. Since the internal fluid keeps interacting with the pipe wall, the changes in the fluid field will keep changing the dynamic behavior of a pipeline system. Conversely, the change in the dynamic behavior of the pipeline system will change the internal fluid field. Sometimes such a structure–fluid interaction phenomenon may result in serious vibrations to cause structural failures. Therefore, it is very important to accurately predict the structural dynamic characteristics of a pipeline and the fluid transients inside of the pipeline during the early design phase. For this, one may need more accurate and realistic pipe-dynamics theory in which the structure–fluid coupling is taken into account, together with using a more accurate solution method.

There have been extensive studies on the modeling and analysis of the flow-induced vibrations of pipeline systems over the past half-century: an extensive review on this subject can be found in Païdoussis and Li (1993). Ashley and Haviland (1950) was the first to consider the internal flow-induced transverse vibration of a pipeline. Since Housner

---

\*Corresponding author. Tel.: +82 32 860 7318; fax: +82 32 866 1434.

*E-mail address:* ulee@inha.ac.kr (U. Lee).

(1952) took into account the Coriolis acceleration of the internal fluid, numerous modified and improved pipe-dynamics theories have been appeared in the literature. They include the linear theories, for instance, by Nemat-Nasser et al. (1966), Stein and Tobriner (1970), Chen (1971), Hill and Davis (1974), Païdoussis et al. (1986), and Lesmez et al. (1990), and the nonlinear theories, for instance, by Semler et al. (1994), Lin and Tsai (1997), Jensen (1997), Zhang et al. (1999), Öz (2001), Lee and Chung (2002). In most existing pipe-dynamics theories, the structural vibration of the pipeline itself has been the main concern and the transient dynamics of internal fluid, which should be coupled with the structural vibration, has been neglected. Mostly, the effect of internal fluid on the pipeline vibration has been taken into account by considering the internal fluid velocity or pressure simply as a known parameter, rather than unknown variables.

To consider the coupling between the pipeline vibration and unsteady internal flow, Lee et al. (1995) derived a set of coupled pipe-dynamics equations for the axial, radial, and transverse vibrations of pipeline, as well as for the transients of unsteady internal fluid pressure and velocity. The coupled pipe-dynamics equations were further generalized by including the circumferential strain effect caused by the internal fluid pressure (Lee and Kim, 1999) and, later on, by including the radial shell vibration and initial axial tension (Gorman et al., 2000). Recently, the vibration of an artery-like tube conveying pulsatile fluid flow was studied by Zhang et al. (2002), and later they showed that the effect of external vibration on the fluid flow rate and pressure in the tube is small (Zhang et al., 2003). The intensive review on the fluid–structure interactions for the slender structures and axial flow can be found in the two-volume book by Païdoussis (1998, 2003).

In the literature, various solution methods have been applied to the pipe-dynamics problems: the classical modal analysis (Housner, 1952; Lee et al., 1995; Jensen, 1997), the Galerkin method (Nemat-Nasser et al., 1966; Chen, 1971; Païdoussis et al., 1986; Lee and Chung, 2002), the Fourier and Laplace transform method (Stein and Tobriner, 1970), the transfer matrix method (Lesmez et al., 1990), the finite element method (FEM) (Hill and Davis, 1974; Lin and Tsai, 1997; Zhang et al., 1999), the finite difference method (Gorman et al., 2000), the method of characteristics (Gorman et al., 2000), the method of multiple scales (Öz, 2001), and the wave approach (Koo and Park, 1998).

The vibrating shape of a structure varies as the frequency of vibration varies. Thus, the conventional finite element model formulated by using the (frequency-independent) polynomial shape functions may require the subdivision of a structure element into finer elements in order to improve the solution accuracy, especially at high frequency. However, if the frequency-dependent (dynamic) shape functions are adopted to formulate the finite element model, such a finer subdivision may not be necessary. This idea leads to the *exact* dynamic stiffness matrix method (Banerjee, 1997). Because the exact dynamic stiffness matrix is the stiffness matrix formulated in the frequency-domain, they can be readily assembled by using the exactly same method that used in the conventional FEM.

In the literature, the fast Fourier transform (FFT)-based dynamic stiffness matrix method is often named *spectral element method* (SEM) [e.g., Doyle (1997), Lee et al. (2000), Lee (2004)]. Because the *exact* dynamic stiffness matrix is formulated from the *exact* dynamic shape functions which satisfy the governing equations of motion, it represents the dynamic behavior of a structural element *exactly*. Thus, the SEM is often justifiably referred to as an exact solution method (Banerjee, 1997; Doyle, 1997; Lee, 2004). Accordingly, in contrast with the conventional FEM, the SEM enables one to use only one finite element for a uniform structural member, regardless of its length, without requiring any further subdivision of the structural member to improve the solution accuracy. This may reduce the number of total degrees of freedom (dof) to significantly lower the computation cost. Lee and Oh (2003) seems to be the first to apply the SEM to the transverse and axial vibrations of a pipeline conveying internal steady fluid. To the authors' best knowledge, the SEM application to the pipeline conveying unsteady flow has not yet been reported in the literature.

Thus, the purposes of the present paper are (i) to develop a spectral element model for the pipeline systems conveying internal unsteady fluid, and (ii) to conduct the FFT-based spectral element analysis to investigate the structural dynamic characteristics and the internal fluid transients of an example pipeline problem.

## 2. Pipe-dynamics equations

We consider a straight pipeline subject to a small amplitude vibration. Fig. 1 shows an infinitesimal pipe-fluid element that can be decomposed into the pipeline element and the fluid element (control volume). In Fig. 1,  $w(x, t)$  and  $u(x, t)$  are the transverse and axial displacements of the pipeline, respectively, and  $p(x, t)$  and  $c(x, t)$  are the fluid pressure and velocity, respectively. The flow-induced resultant normal and tangential forces acting on the pipe wall are indicated by  $N$  and  $\tau S$ , respectively, where  $\tau$  is the shear stress due to the fluid friction and  $S$  is the inner perimeter of pipeline. As shown in Fig. 1(a), the straight pipeline can be assumed to be initially inclined with the angle  $\theta$  (deg) with respect to the ground. The acceleration of gravity, of which direction is perpendicular to the ground, is represented by  $g$ .

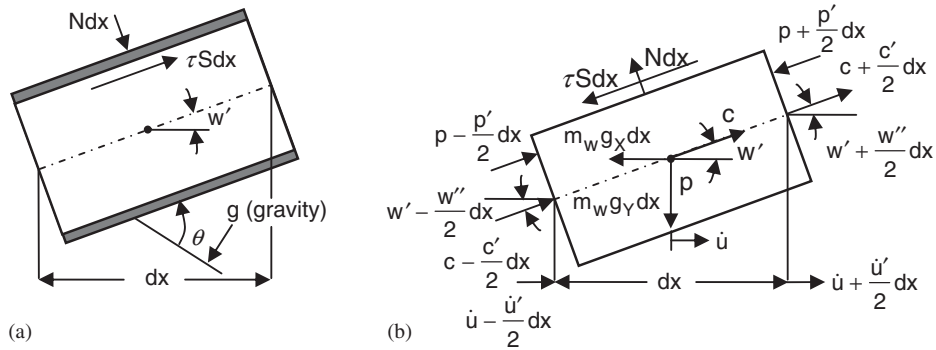


Fig. 1. Free-body diagrams for the (a) pipeline element and (b) fluid elements.

The equations of motion for a pipeline and the relevant boundary conditions can be derived from Hamilton’s principle:

$$\int_{t_2}^{t_1} (\delta T - \delta U + \delta W) dt = 0. \tag{1}$$

The kinetic energy  $T$  and the potential energy  $U$  for the pipeline are given by

$$T = \frac{m_p}{2} \int_0^L (\dot{u}^2 + \dot{w}^2) dx, \tag{2}$$

$$U = \frac{EA_p}{2} \int_0^L \left[ \frac{T_o}{EA_p} + \left( u' + \frac{1}{2}u'^2 + \frac{1}{2}w'^2 \right) \right]^2 dx + \frac{EI_p}{2} \int_0^L w''^2 dx,$$

where the overdot and prime denote the derivatives with respect to the time  $t$  and spatial coordinate  $x$ , respectively.  $E$  is the Young’s modulus and  $T_o$  is the constant axial tension.  $L$ ,  $A_p$ ,  $I_p$ , and  $m_p$  are the length, the cross-sectional area, the second moment of area, and the mass density per length of the pipeline, respectively.

The total virtual work  $\delta W$ , done by the flow-induced forces acting on the pipe wall and the resultant forces and moments applied at the boundaries, is given by

$$\delta W = \int_0^L [(\tau S + Nw')\delta u + (\tau Sw' - N)\delta w] dx + (T_1 - T_o)\delta u(0) + (T_2 + T_o)\delta u(L) + M_1\delta w'(0) + M_2\delta w'(L) + V_1\delta w(0) + V_2\delta w(L), \tag{3}$$

where  $M_1$ ,  $V_1$  and  $T_1$  are the resultant moment, the transverse shear force, and the axial force applied at the inlet boundary  $x = 0$ , respectively, whereas  $M_2$ ,  $V_2$  and  $T_2$  are those applied at the outlet boundary  $x = L$ .

Introducing Eqs. (2) and (3) into Hamilton’s principle and integrating by parts gives the equations of motion for the transverse and axial vibrations of the pipeline as

$$EI_p w'''' - T_o w'' + m_p \ddot{w} - \tau S w' + N = 0, \tag{4}$$

$$(EA_p + T_o)u'' - m_p \ddot{u} + \tau S + Nw' = 0$$

with the boundary conditions at  $x = 0$  as

$$M(0) = M_1 \quad \text{or} \quad w'(0) = 0, \tag{5}$$

$$V(0) = V_1 \quad \text{or} \quad w(0) = 0, \tag{5}$$

$$T(0) = T_1 \quad \text{or} \quad u(0) = 0 \tag{5}$$

and at  $x = L$  as

$$M(L) = M_2 \quad \text{or} \quad w'(L) = 0, \tag{6}$$

$$V(L) = V_2 \quad \text{or} \quad w(L) = 0, \tag{6}$$

$$T(L) = T_2 \quad \text{or} \quad u(L) = 0, \tag{6}$$

where

$$\begin{aligned} M(x) &= EI_p w''(x), \\ V(x) &= -EI_p w'''(x) + T_o w'(x), \\ T(x) &= (EA_p + T_o) u'(x). \end{aligned} \quad (7)$$

By applying Newton's law of motion to the control volume (fluid element) shown in Fig. 1(b), the momentum equations of fluid can be derived as

$$\begin{aligned} (pA)' + Nw' + \tau S + m_w(g_X + \ddot{u} + \dot{c} + cc' + c\dot{u}') &= 0, \\ (pAw')' - N + \tau Sw' + m_w(g_Y + \ddot{w} + 2c\dot{w}' + \dot{c}w' + c^2 w'' + cc'w') &= 0, \end{aligned} \quad (8)$$

where  $m_w$  is the fluid mass density per length,  $g_X = g \sin \theta$  and  $g_Y = g \cos \theta$ . Since the gravity of fluid will become important when the pipeline is inclined as shown in Fig. 1, the gravity effect is included in the momentum equations of the fluid, while it is neglected in the dynamic equations of motion for the pipeline.

Similarly, by applying the law of mass conservation to the control volume, the continuity equation of the fluid can be expressed as

$$\dot{p}A + m_w a^2 (c' - 2v\dot{u}') = 0, \quad (9)$$

where  $a$  is the wave speed of fluid defined by

$$a^2 = \frac{E_v E t}{\rho_w (E_v D + E t)}. \quad (10)$$

In Eq. (10)  $D$  and  $t$  are the inner diameter and thickness of the pipeline, respectively, and  $\rho_w$  and  $E_v$  are the mass density and bulk modulus of the fluid, respectively.

One may readily eliminate the fluid–structure interaction forces  $N$  and  $\tau S$  by properly combining Eqs. (6) and (8) and using the relation (Hansen, 1967)

$$\tau S = m_w \frac{f}{2D} c^2, \quad (11)$$

where  $f$  is the Darcy–Weisbach friction factor. Furthermore, neglecting the convective terms, the small nonlinear terms and the static transverse deflection due to gravity on the fluid may give two equations of motion for the pipeline:

$$\begin{aligned} EI_p w'''' + (pA - T_o + m_w c^2) w'' + p' A w' + m_w (2c\dot{w}' + \dot{c}w' + cc'w') + m\ddot{w} &= 0, \\ (EA_p + T_o) u'' - m_p \ddot{u} + m_w g_Y w' + m_w \frac{f}{2D} c^2 &= 0 \end{aligned} \quad (12)$$

and two fluid dynamics equations for the internal fluid:

$$\begin{aligned} \dot{p}A + a^2 m_w (c' - 2v\dot{u}') &= 0, \\ p' A + m_w g_Y w' + m_w \frac{f}{2D} c^2 + m_w (g_X + \ddot{u} + \dot{c} + cc' + c\dot{u}') &= 0, \end{aligned} \quad (13)$$

where  $m = m_p + m_w$ . The two fluid dynamics equations, Eq. (13), can be combined to obtain a wave equation for the fluid velocity  $c$ . Eq. (13) can be then replaced by

$$\begin{aligned} c'' - \frac{1}{a^2} \dot{c}c' - \frac{1}{a^2} c\dot{c}' - \frac{1}{a^2} \ddot{c} - \frac{f}{a^2 D} c\dot{c} - \frac{g_Y}{a^2} \dot{w}' - 2v\dot{u}'' - \frac{1}{a^2} \dot{c}\dot{u}' - \frac{1}{a^2} c\ddot{u}' &= 0, \\ \dot{p}A + a^2 m_w (c' - 2v\dot{u}') &= 0. \end{aligned} \quad (14)$$

Eqs. (12) and (14) represent the coupled, nonlinear pipe-dynamics equations for the pipeline conveying internal unsteady fluid.

Now, the coupled, nonlinear pipe-dynamics equations will be linearized about the steady state of internal fluid. Thus, the fluid velocity and pressure are assumed as follows:

$$\begin{aligned} c(x, t) &= c_o + c_d(x, t), \\ p(x, t) &= p_o + p_d(x, t), \end{aligned} \quad (15)$$

where  $c_d(x, t) < c_o$  and  $p_d(x, t) < p_o$  represent the small perturbations with respect to constant steady-state values  $c_o$  and  $p_o$ , respectively. Substituting Eq. (15) into Eqs. (12) and (14) and neglecting small nonlinear terms may give the linear,

semi-coupled pipe-dynamics equations as follows:

$$EI_p w'''' + (p_o A - T_o + m_w c_o^2) w'' + 2m_w c_o \dot{w}' + m \ddot{w} = 0, \tag{16a}$$

$$(EA_p + T_o) u'' - m_p \ddot{u} + m_w g_Y w' + m_w \frac{f}{D} c_o c_d + m_w \frac{f}{2D} c_o^2 = 0, \tag{16b}$$

$$c_d'' - \frac{c_o}{a^2} \dot{c}_d' - \frac{f}{a^2 D} c_o \dot{c}_d - \frac{\ddot{c}_d}{a^2} - \frac{g_Y}{a^2} \dot{w}' - 2\nu \dot{u}'' - \frac{c_o}{a^2} \ddot{u}' = 0, \tag{16c}$$

$$\dot{p}_d A + a^2 m_w (c_d' - 2\nu \dot{u}') = 0. \tag{16d}$$

One may see from Eq. (16), that the transverse displacement  $w(x, t)$  and the perturbed fluid pressure  $p_d(x, t)$  are completely decoupled from the other variables, the axial displacement  $u(x, t)$  and the perturbed fluid velocity  $c_d(x, t)$ . Thus, once  $w(x, t)$  is determined from Eq. (16a),  $u(x, t)$  and  $c_d(x, t)$  can be solved from two coupled equations Eqs. (16b) and (16c), followed by determining  $p_d(x, t)$  from Eq. (16d).

### 3. Formulation of spectral element matrix

The general solutions of Eq. (16) can be assumed in the spectral forms (Doyle, 1997; Lee, 2004)

$$\begin{aligned} w(x, t) &= \sum_{n=1}^N W_n(x) e^{i\omega_n t}, & u(x, t) &= \sum_{n=1}^N U_n(x) e^{i\omega_n t}, \\ c_d(x, t) &= \sum_{n=1}^N C_n(x) e^{i\omega_n t}, & p_d(x, t) &= \sum_{n=1}^N P_n(x) e^{i\omega_n t}, \end{aligned} \tag{17}$$

where  $i = \sqrt{-1}$  and  $\omega_n = 2\pi n/T$  ( $n = 1, 2, \dots, N$ ) represent the discrete frequencies:  $T$  is the period (i.e., time window) and  $N$  is the total number of spectral components to be considered in the FFT-based spectral analysis. In Eq. (7),  $W_n(x)$ ,  $U_n(x)$ ,  $C_n(x)$  and  $P_n(x)$  represent the spatially dependent spectral components (or Fourier coefficients) of  $w(x, t)$ ,  $u(x, t)$ ,  $c_d(x, t)$  and  $p_d(x, t)$ , respectively. Once the spectral components  $W_n(x)$ ,  $U_n(x)$ ,  $C_n(x)$  and  $P_n(x)$  are computed, the vibration responses in the time-domain (i.e.,  $w(x, t)$ ,  $u(x, t)$ ,  $c_d(x, t)$  and  $p_d(x, t)$ ) can be reconstructed by summing all computed spectral components, as self-explained by Eq. (17). This reconstruction process can be performed very efficiently by using the FFT algorithm. The summation and the subscript  $n$  used in Eq. (17) are so obvious that they will be omitted in the following for brevity.

Substituting Eq. (17) into Eq. (16) yields

$$\begin{aligned} a_1 W'''' + a_2 W'' + a_3 i\omega W' - a_4 \omega^2 W &= 0, \\ b_1 U'' - b_2 \omega^2 U + b_3 W' + b_4 C + b_5 &= 0, \\ C'' + c_1 i\omega C' + (c_2 i\omega - c_3 \omega^2) C + c_4 i\omega W' + c_5 i\omega U'' - c_1 \omega^2 U' &= 0, \\ i\omega P + d_1 (C' + c_5 i\omega U') &= 0, \end{aligned} \tag{18}$$

where

$$\begin{aligned} a_1 &= EI_p, & a_2 &= p_o A - T_o + m_w c_o^2, & a_3 &= 2m_w c_o, & a_4 &= m, \\ b_1 &= EA_p + T_o, & b_2 &= -m_p, & b_3 &= m_w g_Y, & b_4 &= m_w c_o f/D, & b_5 &= m_w c_o^2 f/2D, \\ c_1 &= -c_o/a^2, & c_2 &= -c_o f/(a^2 D), & c_3 &= -1/a^2, & c_4 &= -g_Y/a^2, & c_5 &= -2\nu, \\ d_1 &= \rho_w a^2. \end{aligned} \tag{19}$$

In general, the spectral element matrix is formulated from the homogeneous governing equations (Doyle, 1997; Lee, 2004), which can be reduced from Eq. (18) as

$$\begin{aligned} a_1 W'''' + a_2 W'' + a_3 i\omega W' - a_4 \omega^2 W &= 0, \\ b_1 U'' - b_2 \omega^2 U + b_3 W' + b_4 C &= 0, \\ C'' + c_1 i\omega C' + (c_2 i\omega - c_3 \omega^2) C + c_4 i\omega W' + c_5 i\omega U'' - c_1 \omega^2 U' &= 0, \\ i\omega P + d_1 (C' + c_5 i\omega U') &= 0. \end{aligned} \tag{20}$$

The general solutions of Eq. (20) are assumed as

$$\begin{aligned} W(x) &= \bar{W}e^{ikx}, & U(x) &= \bar{U}e^{ikx}, \\ C(x) &= \bar{C}e^{ikx}, & P(x) &= \bar{P}e^{ikx}, \end{aligned} \quad (21)$$

where  $k$  is the wavenumber.

Substituting Eq. (21) into Eq. (20) gives an eigenvalue problem as

$$\begin{bmatrix} K_{11} & 0 & 0 \\ K_{21} & K_{22} & K_{23} \\ K_{31} & K_{32} & K_{33} \end{bmatrix} \begin{Bmatrix} \bar{W} \\ \bar{U} \\ \bar{C} \end{Bmatrix} = \begin{Bmatrix} 0 \\ 0 \\ 0 \end{Bmatrix}, \quad (22)$$

where

$$\begin{aligned} K_{11} &= a_1k^4 - a_2k^2 - a_3\omega k - a_4\omega^2, & K_{21} &= b_3ik, \\ K_{22} &= -b_1k^2 - b_2\omega^2, & K_{23} &= b_4, \\ K_{31} &= -c_4\omega k, & K_{32} &= -(c_5i\omega k^2 + c_1\omega^2ik), \\ K_{33} &= -k^2 - c_1\omega k + c_2i\omega - c_3\omega^2. \end{aligned} \quad (23)$$

From the condition for the existence of nontrivial solutions of Eq. (22), one may obtain the dispersion equations as

$$\begin{aligned} a_1k^4 - a_2k^2 - a_3\omega k - a_4\omega^2 &= 0, \\ b_1k^4 + b_1c_1\omega k^3 + \{(b_2 + b_1c_3)\omega^2 - i(b_1c_2 - b_4c_5)\omega\}k^2 \\ + (b_2c_1\omega^3 + ib_4c_1\omega^2)k + b_2(c_3\omega - ic_2)\omega^3 &= 0. \end{aligned} \quad (24)$$

The first dispersion equation, Eq. (24a), will provide four wavenumbers  $k_1, k_2, k_3$  and  $k_4$  for the bending vibration modes, whereas the second dispersion equation, Eq. (24b), will provide four wavenumbers  $k_5, k_6, k_7$  and  $k_8$  for the axial vibration–fluid velocity coupling modes.

Using the eight wavenumbers obtained from Eq. (24), the general solutions of Eq. (20) can be expressed as

$$\begin{aligned} W(x) &= \sum_{j=1}^4 \bar{W}_j e^{ik_j x} = [\mathbf{e}_w(x)]\{\boldsymbol{\phi}_w\}, \\ U(x) &= \sum_{j=1}^4 \bar{U}_j e^{ik_{j+4} x} = [\mathbf{e}_{uc}(x)]\{\boldsymbol{\phi}_{uc}\}, \\ C(x) &= \sum_{j=1}^4 \alpha_j \bar{U}_j e^{ik_{j+4} x} = [\mathbf{e}_{uc}(x)][\mathbf{D}_{uc}]\{\boldsymbol{\phi}_{uc}\}, \end{aligned} \quad (25)$$

where

$$\begin{aligned} [\mathbf{e}_w(x)] &= [e^{ik_1 x} \quad e^{ik_2 x} \quad e^{ik_3 x} \quad e^{ik_4 x}], \\ [\mathbf{e}_{uc}(x)] &= [e^{ik_5 x} \quad e^{ik_6 x} \quad e^{ik_7 x} \quad e^{ik_8 x}], \\ [\mathbf{D}_{uc}] &= [\text{diag}(\alpha_j)] \quad (j = 1, 2, 3, 4) \end{aligned} \quad (26)$$

and  $\{\boldsymbol{\phi}_w\}$  and  $\{\boldsymbol{\phi}_{uc}\}$  are constant vectors. In Eq. (26),  $[\text{diag}(\alpha_j)]$  denotes the diagonal matrix and its  $j$ th component is defined by

$$\alpha_j = -\frac{K_{22}(k = k_{j+4})}{K_{23}(k = k_{j+4})} \quad (j = 1, 2, 3, 4). \quad (27)$$

Now, consider a finite pipeline element of length  $l$ . The spectral components of the nodal dof (simply, spectral nodal dofs), shown in Fig. 2, are defined by

$$\begin{aligned} W(0) &= W_1, & W(l) &= W_2, \\ \Theta(0) &= \Theta_1, & \Theta(l) &= \Theta_2, \\ U(0) &= U_1, & U(l) &= U_2, \\ C(0) &= C_1, & C(l) &= C_2, \\ P(0) &= P_1, & P(l) &= P_2, \end{aligned} \quad (28)$$

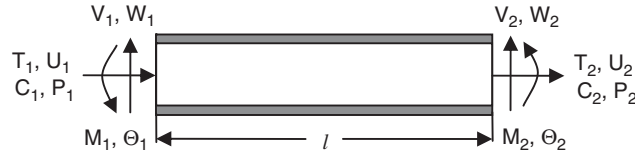


Fig. 2. Sign convention for the pipeline element.

where  $\Theta(x) = W'(x)$  denotes the slope. Substituting Eq. (25) into Eq. (28) gives the relationships between the spectral nodal degrees of freedom (dofs) vectors and the constants vectors as follows:

$$\begin{aligned} \{d_w\} &= [H_w(\omega)]\{\phi_w\}, \\ \{d_{uc}\} &= [H_{uc}(\omega)]\{\phi_{uc}\}, \end{aligned} \tag{29}$$

where

$$\begin{aligned} \{d_w\} &= \{W_1 \quad \theta_1 \quad W_2 \quad \theta_2\}^T, \\ \{d_{uc}\} &= \{U_1 \quad U_2 \quad C_1 \quad C_2\}^T, \end{aligned}$$

$$\begin{aligned} [H_w(\omega)] &= \begin{bmatrix} 1 & 1 & 1 & 1 \\ ik_1 & ik_2 & ik_3 & ik_4 \\ e_1 & e_2 & e_3 & e_4 \\ ik_1e_1 & ik_2e_2 & ik_3e_3 & ik_4e_4 \end{bmatrix}, \\ [H_{uc}(\omega)] &= \begin{bmatrix} 1 & 1 & 1 & 1 \\ e_5 & e_6 & e_7 & e_8 \\ \alpha_1 & \alpha_2 & \alpha_3 & \alpha_4 \\ \alpha_1e_5 & \alpha_2e_6 & \alpha_3e_7 & \alpha_4e_8 \end{bmatrix}, \end{aligned} \tag{30}$$

with

$$e_j = e^{ik_j l} \quad (j = 1, 2, 3, \dots, 8). \tag{31}$$

From Eq. (29), one may obtain

$$\begin{aligned} \{\phi_w\} &= [H_w(\omega)]^{-1}\{d_w\}, \\ \{\phi_{uc}\} &= [H_{uc}(\omega)]^{-1}\{d_{uc}\}. \end{aligned} \tag{32}$$

Substituting Eq. (32) into Eq. (25) gives

$$\begin{aligned} W(x) &= [N_w(x; \omega)]\{d_w\}, \\ U(x) &= [N_u(x; \omega)]\{d_{uc}\}, \\ C(x) &= [N_c(x; \omega)]\{d_{uc}\}, \end{aligned} \tag{33}$$

where  $[N_w]$ ,  $[N_u]$  and  $[N_c]$  are the dynamic (frequency-dependent) shape function matrices defined by

$$\begin{aligned} [N_w(x; \omega)] &= [e_w(x)][H_w(\omega)]^{-1}, \\ [N_u(x; \omega)] &= [e_{uc}(x)][H_{uc}(\omega)]^{-1}, \\ [N_c(x; \omega)] &= [e_{uc}(x)][H_{uc}(\omega)][H_{uc}(\omega)]^{-1}. \end{aligned} \tag{34}$$

The variational approach will be used to formulate the spectral element matrix by using the displacement and fluid field given by Eq. (33). The weak form statements of the first three equations of Eq. (18) are given by

$$\begin{aligned} \int_0^l \{a_1 W'' \delta W'' + (a_2 + T_o) W'' \delta W + T_o W' \delta W' + a_3 i \omega W' \delta W - a_4 \omega^2 W \delta W\} dx \\ - V_2 \delta W_2 - V_1 \delta W_1 - M_2 \delta \Theta_2 - M_1 \delta \Theta_1 = 0, \end{aligned}$$

$$\begin{aligned} & \int_0^l (b_1 U' \delta U' + b_2 \omega^2 U \delta U - b_3 W' \delta U - b_4 C \delta U - b_5 \delta U) dx \\ & - T_2 \delta U_2 - T_1 \delta U_1 = 0, \\ & \int_0^l \{-C' \delta C' + c_1 i \omega C' \delta C + (c_2 i \omega - c_3 \omega^2) C + c_4 i \omega W' \delta C - c_5 i \omega U' \delta C' - c_1 \omega^2 U' \delta C\} dx \\ & + (i \omega P_2 / d_1) \delta C_2 - (i \omega P / d_1) \delta C_1 = 0. \end{aligned} \tag{35}$$

where  $M_i$ ,  $V_i$  and  $T_i$  ( $i = 1, 2$ ) represent the spectral components of the resultant moments, the transverse shear forces and the axial forces, respectively, at two nodes  $x = 0$  and  $x = l$ , as defined by Eq. (5). Similarly,  $W_i, \theta_i, U_i, C_i$  and  $P_i$  ( $i = 1, 2$ ) represent the spectral nodal dofs at two nodes  $x = 0$  and  $x = l$ , as defined in Eq. (28). Eq. (18d) has been used to obtain Eq. (35c).

Substituting Eq. (34) into Eq. (35) and taking some manipulation gives a matrix form of equation as

$$[S(\omega)]\{d\} = \{f\}, \tag{36}$$

where  $\{d\}$  and  $\{f\}$  are the spectral nodal dofs vector and the spectral nodal forces vector, respectively, defined by

$$\{d\} = \begin{Bmatrix} W_1 \\ \theta_1 \\ W_2 \\ \theta_2 \\ U_1 \\ U_2 \\ C_1 \\ C_2 \end{Bmatrix}, \quad \{f\} = \begin{Bmatrix} V_1 \\ M_1 \\ V_2 \\ M_2 \\ T_1 \\ T_2 \\ -i \omega P_1 / d_1 \\ i \omega P_2 / d_1 \end{Bmatrix} + \begin{Bmatrix} 0 \\ 0 \\ 0 \\ 0 \\ \int_0^l b_5 [N_u]^T dx \\ \vdots \end{Bmatrix}_{4 \times 1}, \tag{37}$$

and  $[S(\omega)]$  is the spectral element matrix defined by

$$[S(\omega)] = \begin{bmatrix} s_{11} & \mathbf{0} \\ s_{21} & s_{22} \end{bmatrix}, \tag{38}$$

where

$$\begin{aligned} [s_{11}] &= \int_0^l \{a_1 [N_w'']^T [N_w''] + \bar{a}_2 [N_w]^T [N_w''] + T_o [N_w']^T [N_w'] + a_3 i \omega [N_w]^T [N_w'] \\ & - a_4 \omega^2 [N_w]^T [N_w]\} dx, \\ [s_{21}] &= \int_0^l \{-b_3 [N_u]^T [N_w'] - c_4 i \omega [N_c]^T [N_w']\} dx, \\ [s_{22}] &= \int_0^l \{b_1 [N_u']^T [N_u'] + b_2 \omega^2 [N_u]^T [N_u] - b_4 [N_u]^T [N_c] + [N_c']^T [N_c'] - c_1 i \omega [N_c]^T [N_c'] \\ & - (c_2 i \omega - c_3 \omega^2) [N_c]^T [N_c] + c_5 i \omega [N_c']^T [N_u'] + c_1 \omega^2 [N_c]^T [N_u']\} dx, \end{aligned} \tag{39}$$

where

$$\bar{a}_2 = p_o A + m_w c_o^2. \tag{40}$$

In Eq. (38),  $[s_{12}] = \mathbf{0}$ , which simply implies that the transverse displacement is not coupled with the axial displacement and fluid velocity. If the fluid-related terms (2nd and 4th terms) are removed from  $[s_{11}]$ , one may confirm that the symmetric spectral element matrix for the bending vibration of a simple beam without internal flow is recovered (Lee, 2004).

As an important advantage of the spectral-element-matrix-based SEM, as mentioned previously, only one finite element will be enough for a uniform pipeline, regardless of its length, to obtain accurate dynamic characteristics of the pipeline conveying internal unsteady fluid. However, if the pipeline is not uniform in terms of geometry or material properties, then the pipeline needs to be divided into more finite elements. In this case, the spectral element matrices should be assembled and this can be done by using the same assembly techniques as used in the conventional FEM. The major difference is the addition of a Do-Loop over all discrete frequencies. Thus, if  $N$  spectral components are considered in the spectral element analysis as shown in Eq. (17), the problem can be thought as a sequence of  $N$  pseudo-static problems.

Assembling the spectral element Eq. (36) and then applying the appropriate boundary conditions will provide a global system dynamic equation (in frequency domain) as

$$[\mathbf{S}_g(\omega)]\{\mathbf{d}_g(\omega)\} = \{\mathbf{f}_g(\omega)\}, \tag{41}$$

where  $\{\mathbf{f}_g\}$  is the global spectral nodal forces vector,  $\{\mathbf{d}_g\}$  is the global spectral nodal dof vector, and  $[\mathbf{S}_g(\omega)]$  is the global dynamic stiffness matrix. The natural frequencies  $\omega_{\text{nat}}$  of a pipeline system can be obtained from the condition that determinant of  $[\mathbf{S}(\omega)]$  should vanish at the natural frequencies, that is

$$|\mathbf{S}(\omega_{\text{nat}})| = 0. \tag{42}$$

#### 4. Numerical results and discussions

As illustrative examples, two straight pipelines simply supported at both ends are considered. As shown in Fig. 3, pipeline A and pipeline B are both horizontal with respect to the ground, i.e.,  $\theta = 0^\circ$ , subject to same axial tension  $T_o = 82 \text{ N}$ , and have exactly the same geometry. That is, they have a length  $L = 6000 \text{ mm}$ , internal diameter  $D = 32.12 \text{ mm}$ , and thickness  $t = 1.4 \text{ mm}$ . Pipeline A has uniform material properties: Young’s modulus  $E_1 = 117 \text{ GPa}$ , Poisson’s ratio  $\nu_1 = 0.285$  and mass density per unit length  $m_{p1} = 1.318 \text{ kg/m}$ . Pipeline B consists of two materials: the first-half of the pipeline has material properties ( $E_1, \nu_1$  and  $m_{p1}$ ) which are same as those for pipeline A, and the second half of the pipeline B has material properties  $E_2 = 73 \text{ GPa}$ ,  $\nu_2 = 0.330$  and  $m_{p2} = 0.413 \text{ kg/m}$ . The mass density of fluid per unit length is  $m_w = 0.81 \text{ kg/m}$ .

The accuracy of the present spectral element model is evaluated first by comparing the eigenfrequencies obtained by using the present SEM with those obtained by the conventional FEM and the exact theory from Blevins (1979). The finite element model used to obtain the FEM results is summarized in Appendix A.

Table 1 compares the eigenfrequencies of the first four bending vibration modes, the first axial vibration mode, and the first fluid mode for pipeline A, all obtained by the present SEM, FEM, and the exact theory from Blevins (1979). Because pipeline A is uniform, only one finite element is used to obtain the SEM results. On the other hand, the FEM results are improved by increasing the total number of finite elements from 10 to 100, as shown in Table 1. When the (steady-state) flow velocity is  $c_o = 0 \text{ m/s}$ , the eigenfrequencies obtained by the present SEM are exactly identical to the exact theoretical solutions. One can observe from Table 1 that, at all flow velocities, the FEM results tend to converge to the SEM results as the total number of finite elements used in FEM is increased. For the present example problem, one has to use more than 50 finite elements in the FEM to achieve the same accuracy for the fifth eigenfrequency as achieved by the present SEM. One can also observe from Table 1 that the real parts of eigenfrequencies (i.e., natural frequencies) are reduced in magnitude as the fluid velocity  $c_o$  is increased. As a result, the first natural frequency

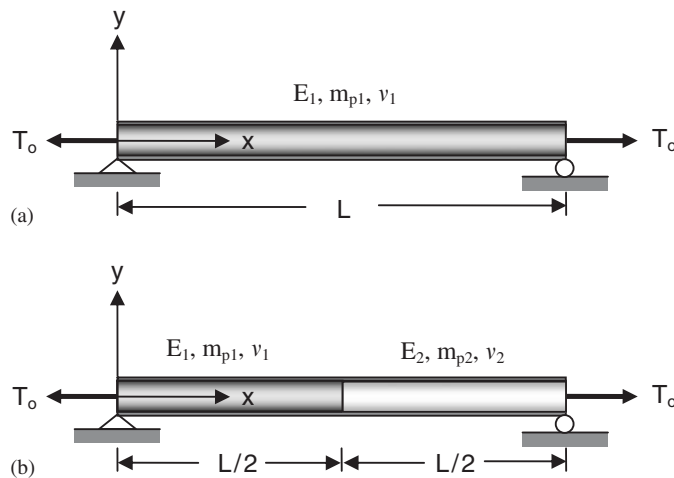


Fig. 3. Example problems: a simply supported straight pipelines conveying internal unsteady fluid, where  $T_o = 82 \text{ N}$ : (a) Pipeline A: uniform pipeline; (b) pipeline B: nonuniform pipeline.

Table 1

Comparison of the eigenfrequencies (Hz) for the uniform pipeline A, obtained by the present SEM, FEM and the exact theory (Blevins, 1979)

Fluid velocity (m/s)	Method	$N$	$\omega_1^{(w)}$	$\omega_2^{(w)}$	$\omega_3^{(w)}$	$\omega_4^{(w)}$	$\omega_6^{(c)}$	$\omega_{12}^{(u)}$
0	Theory (exact)		1.47	5.89	13.26	23.57	51.98	150.73
	SEM	1	1.47	5.89	13.26	23.57	51.98	150.73
	FEM	10	1.47	5.89	13.27	23.61	52.03	157.39
		20	1.47	5.89	13.26	23.58	51.99	150.77
		50	1.47	5.89	13.26	23.58	51.98	150.74
		100	1.47	5.89	13.26	23.57	51.98	150.74
5	SEM	1	1.45	5.87	13.24	23.56	51.98 + 0.26i	150.74 + 0.01i
		10	1.45	5.87	13.25	23.59	52.03 + 0.26i	150.89 + 0.01i
	FEM	20	1.45	5.87	13.24	23.56	51.99 + 0.26i	150.77 + 0.01i
		50	1.45	5.87	13.24	23.56	51.98 + 0.26i	150.74 + 0.01i
		100	1.45	5.87	13.24	23.56	51.98 + 0.26i	150.74 + 0.01i
		10	SEM	1	1.37	5.81	13.18	23.50
10	1.37			5.81	13.19	23.54	52.03 + 0.47i	150.89 + 0.02i
FEM	20		1.37	5.81	13.18	23.50	51.99 + 0.47i	150.77 + 0.02i
	50		1.37	5.81	13.18	23.50	51.98 + 0.47i	150.74 + 0.02i
	100		1.37	5.81	13.18	23.50	51.98 + 0.47i	150.74 + 0.02i
	20		SEM	1	1.03	5.55	12.94	23.26
10		1.03		5.55	12.95	23.30	52.03 + 0.86i	150.89 + 0.03i
FEM		20	1.03	5.55	12.94	23.26	51.99 + 0.86i	150.77 + 0.03i
		50	1.03	5.55	12.94	23.26	51.98 + 0.86i	150.74 + 0.03i
		100	1.03	5.55	12.94	23.26	51.97 + 0.86i	150.74 + 0.03i
		28.65	SEM	1	0.00	5.18	12.59	22.93
10	0.00			5.18	12.60	22.97	52.02 + 1.18i	150.89 + 0.04i
FEM	20		0.00	5.18	12.59	22.93	51.98 + 1.18i	150.77 + 0.04i
	50		0.00	5.18	12.59	22.93	51.97 + 1.18i	150.74 + 0.04i
	100		0.00	5.18	12.59	22.93	51.97 + 1.18i	150.74 + 0.04i

Note:  $N$  = number of finite elements;  $(w)$  = bending vibration mode;  $(u)$  = axial vibration mode;  $(c)$  = fluid mode.

Table 2

Comparison of the eigenfrequencies (Hz) for the nonuniform pipeline B, obtained by the present SEM and FEM when  $c_o = 10$  m/s

Fluid velocity (m/s)	Method	$N$	$\omega_1^{(w)}$	$\omega_2^{(w)}$	$\omega_3^{(w)}$	$\omega_4^{(w)}$	$\omega_6^{(c)}$	$\omega_{12}^{(u)}$
10	SEM	2	1.34	5.97	13.34	24.09	48.45 + 0.46i	150.67 + 0.46i
		10	1.34	5.97	13.35	24.13	48.50 + 0.46i	152.08 + 0.46i
	FEM	20	1.34	5.97	13.34	24.09	48.46 + 0.46i	151.22 + 0.46i
		50	1.34	5.97	13.34	24.09	48.45 + 0.46i	150.73 + 0.46i
		100	1.34	5.97	13.34	24.09	48.45 + 0.46i	150.69 + 0.45i

Note:  $N$  = number of finite elements;  $(w)$  = bending vibration mode;  $(u)$  = axial vibration mode;  $(c)$  = fluid mode.

becomes zero at about  $c_o = 28.65$  m/s (denoted by  $c_D$ ) and a divergence instability occurs. Similarly, Table 2 compares the eigenfrequencies for the nonuniform pipeline B, when  $c_o = 10$  m/s. As pipeline B consists of two uniform beams of different materials, two finite elements are used. One can also confirm that the FEM results indeed converge to the SEM results as the total number of finite elements used in FEM is increased.

Table 3 compares the CPU times (seconds) required to compute the eigenfrequencies by the present SEM and FEM for the uniform pipeline A and the nonuniform pipeline B, given in Tables 1 and 2, when  $c_o = 10$  m/s. The MATLAB function 'eig' is used to compute the FEM results, while a common root-finding approach is used to obtain the SEM results. Table 3 shows that the CPU time for the FEM results increases rapidly as the number of finite elements used in FEM increases over about 20 for the present two example pipelines.

Table 3

Comparison of the CPU times (seconds) required to compute the eigenfrequencies by the present SEM and FEM for the uniform pipeline A and the nonuniform pipeline B, given in Tables 1 and 2 when  $c_o = 10$  m/s

Methods		SEM	FEM		
Uniform pipeline A	$N$	1	10	20	50
	CPU time (s)	65	44	348	12735
Nonuniform pipeline B	$N$	2	10	20	50
	CPU time (s)	75	45	361	13441

Note:  $N$  = number of finite elements.

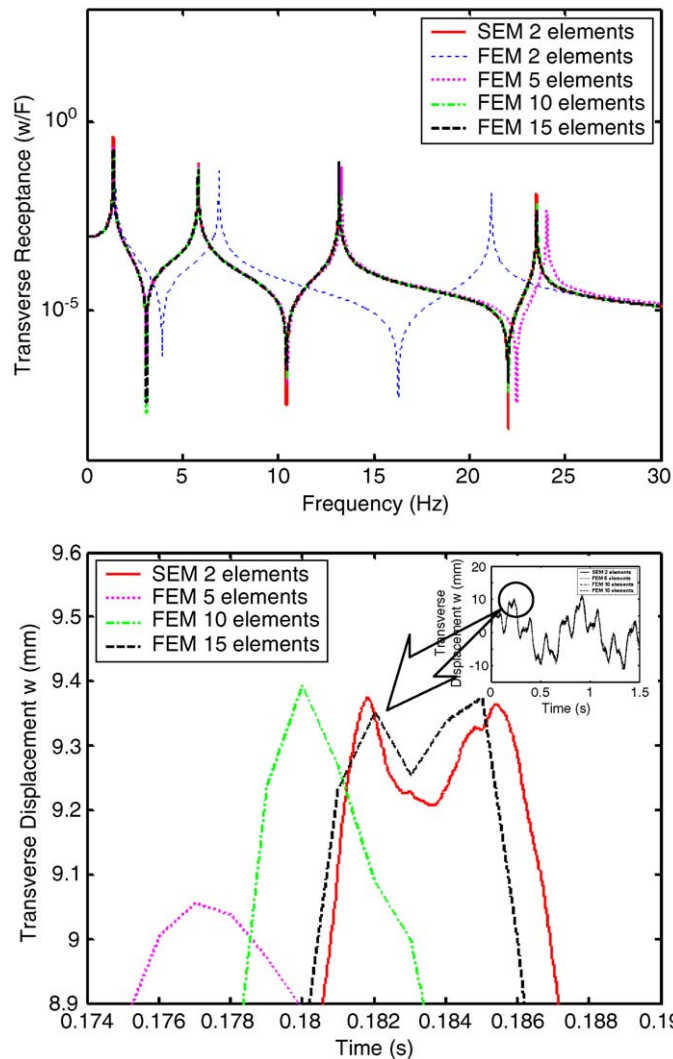


Fig. 4. Comparison of the transverse displacements at  $x = L/5$  in the frequency and time domains obtained by the present SEM and FEM.

The uniform pipeline A, shown in Fig. 3(a), is considered for the results given in Figs. 4–10. Fig. 4 compares the dynamic responses of the transverse displacement obtained by the present SEM and FEM in the frequency- and time-domains. It is assumed that the fluid velocity is  $c_o = 10$  m/s. To excite the pipeline, a point load of 1 kN is applied at

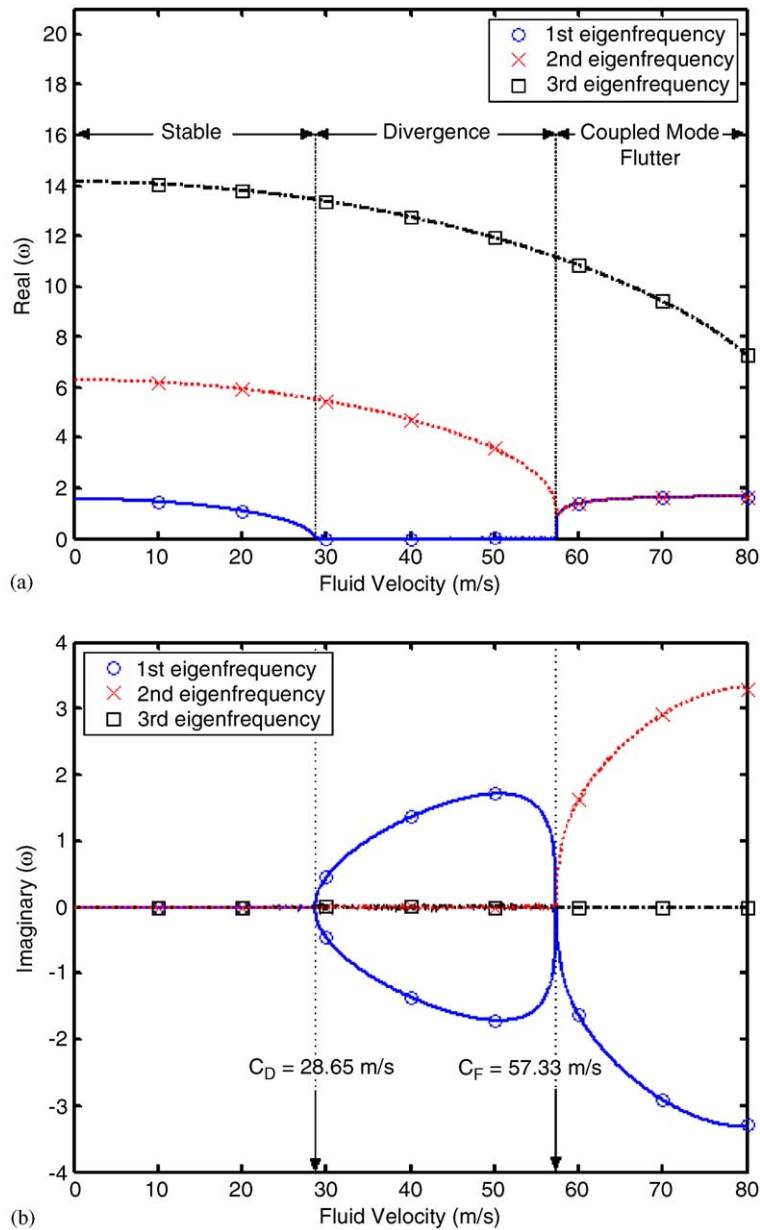


Fig. 5. Effect of fluid velocity on the eigenfrequencies  $\omega$  of the first three bending vibration modes: (a) real part of  $\omega$ ; (b) imaginary part of  $\omega$ .

$x = L/5$  for 0.001 s. The dynamic responses are then computed at the excitation point, *i.e.*,  $x = L/5$ . Due to the existence of the point load, two elements are used for the SEM results. It is certain from Fig. 4 that the dynamic responses obtained by the FEM converge to the SEM results as the total number of finite elements used in the FEM is increased. Thus, the results shown in both Table 1 and Fig. 4 may serve as proof of the high accuracy of the present spectral element model.

Fig. 5 shows the effect of fluid velocity  $c_o$  on the real and imaginary parts of the eigenfrequencies for the first three bending vibration modes. A divergence instability may occur when the imaginary part of an eigenfrequency is negative and the real part is zero, whereas a flutter instability may occur when the imaginary part is negative, but the real part is not zero. For the present example problem, Fig. 5 shows that the divergence instability may occur in the first bending

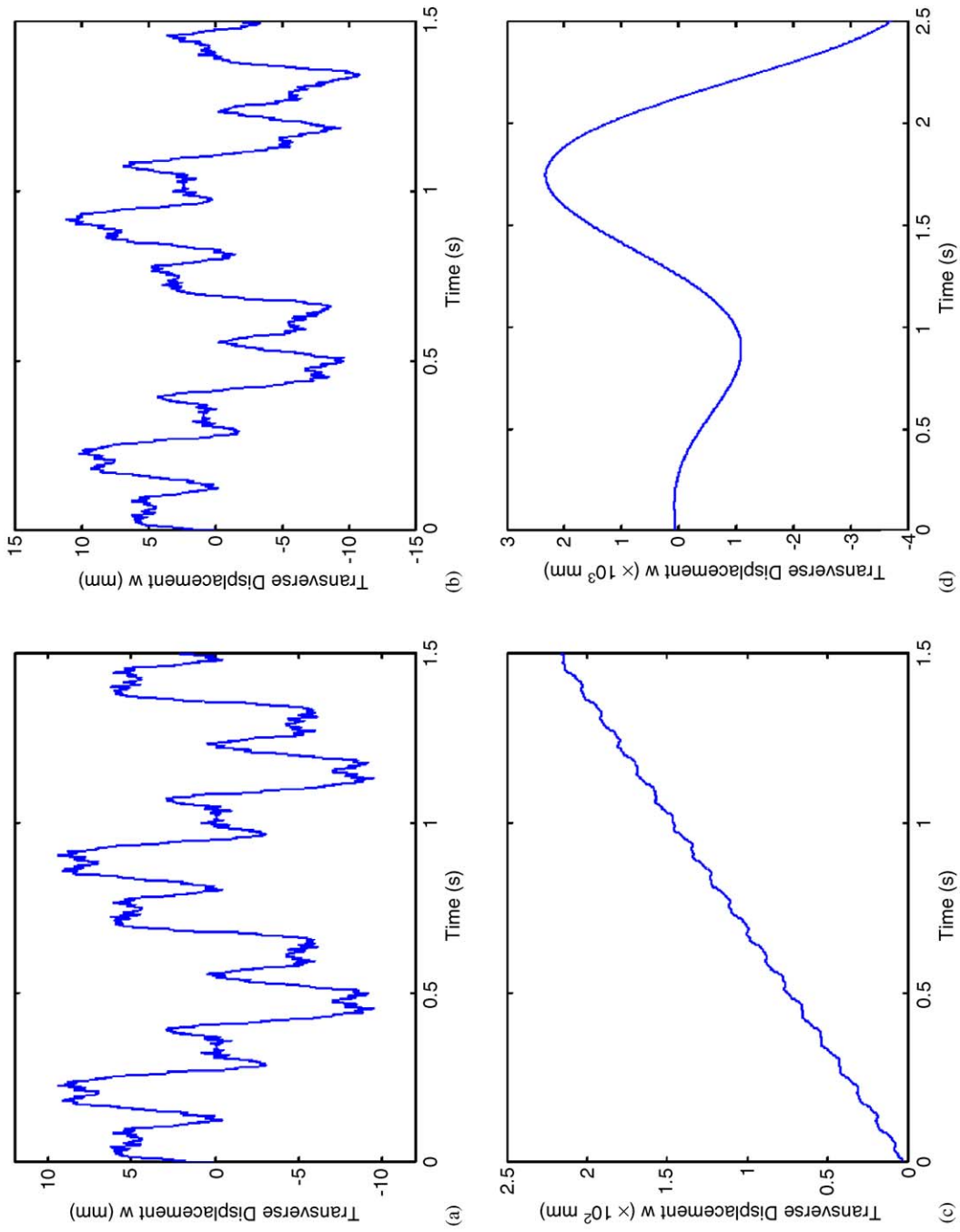


Fig. 6. The transverse displacement of the pipeline at  $x = L/5$  versus the fluid velocity  $c_o$ : (a)  $c_o = 0$  m/s; (b)  $c_o = 10$  m/s; (c)  $c_o = 28.65$  m/s ( $c_P$ ); (d)  $c_o = 57.33$  m/s ( $c_P$ ).

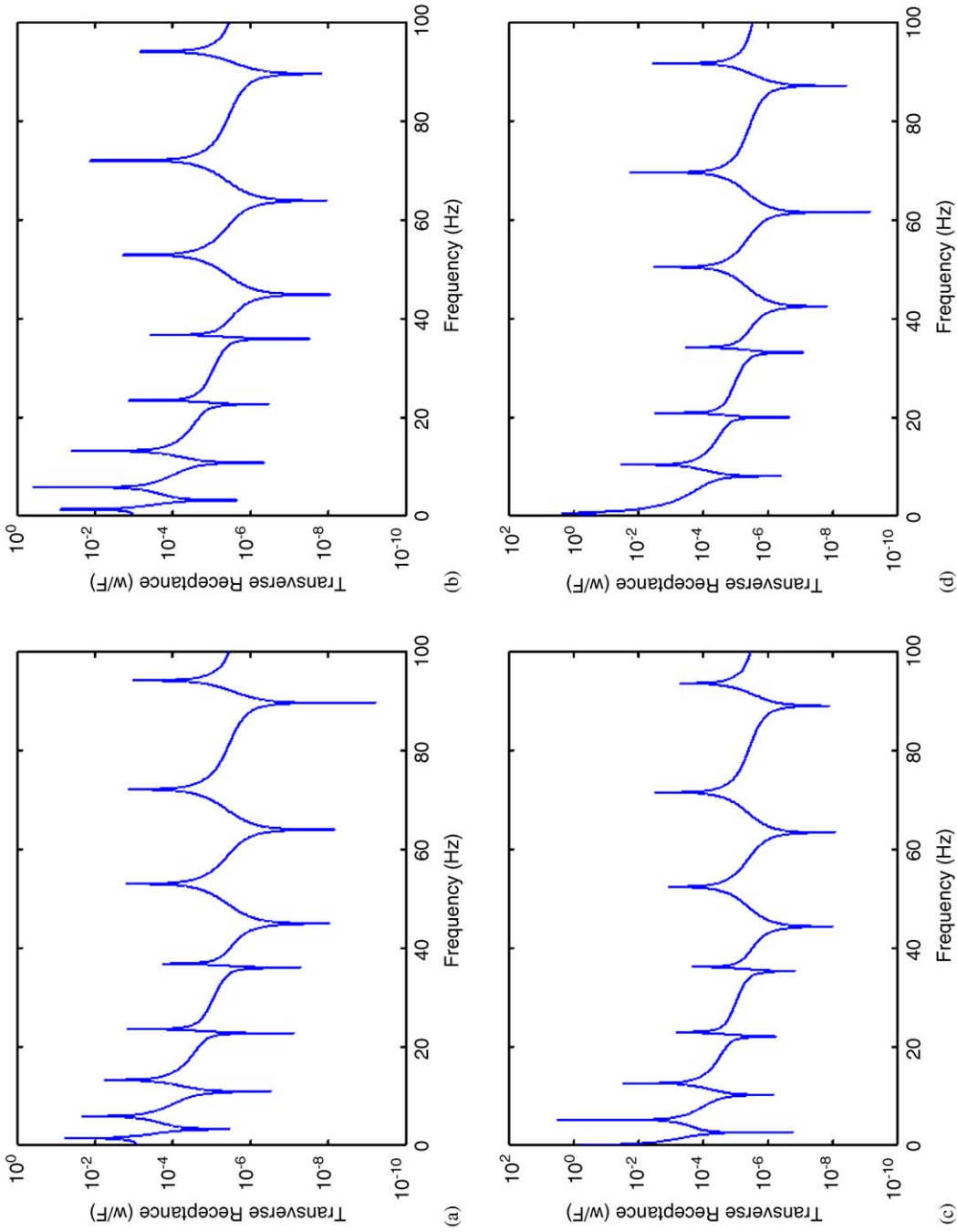


Fig. 7. The transverse receptances of the pipeline at  $x = L/5$  versus the fluid velocity  $c_o$ . (a)  $c_o = 0$  m/s; (b)  $c_o = 10$  m/s; (c)  $c_o = 28.65$  m/s ( $c_D$ ); (d)  $c_o = 57.33$  m/s ( $c_F$ ).

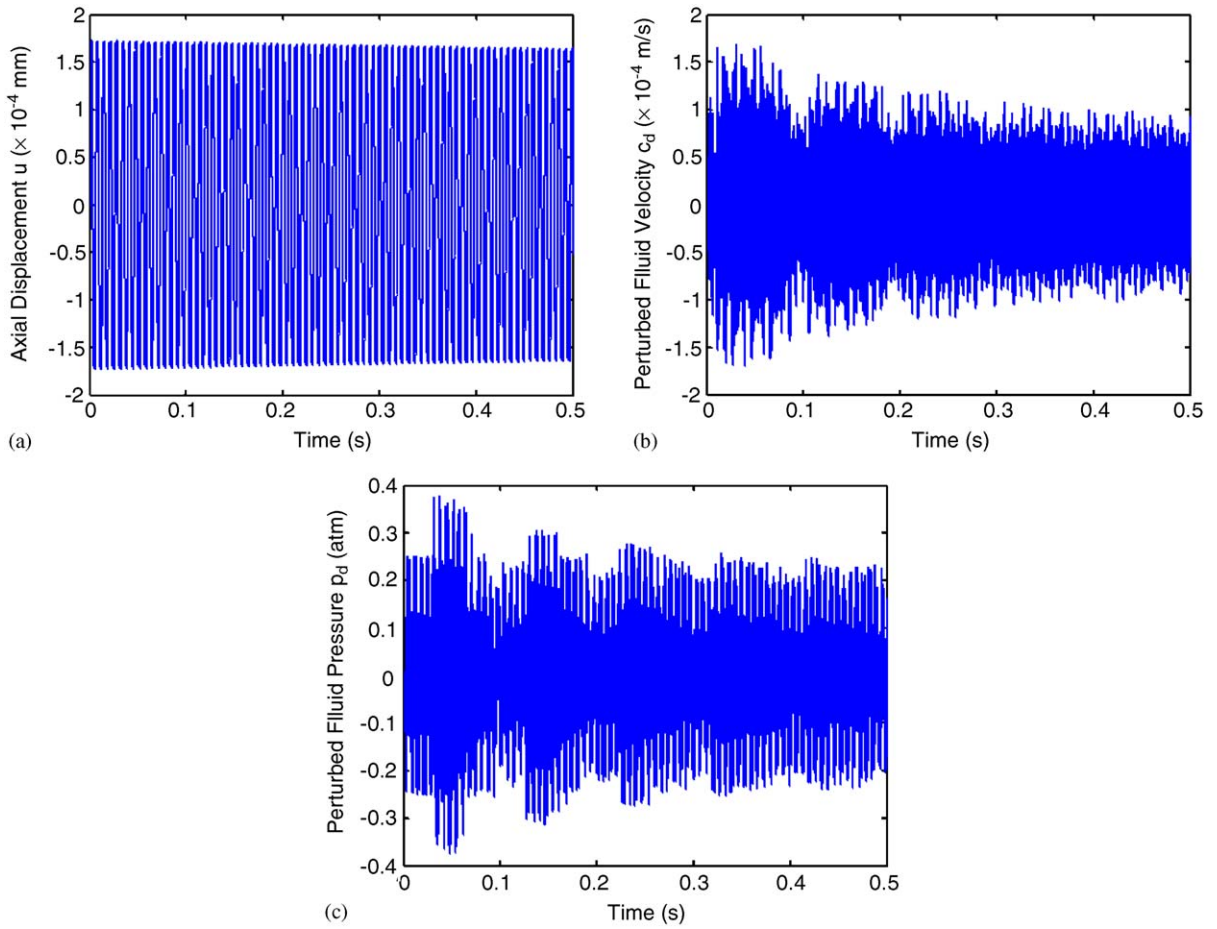


Fig. 8. The axial displacement, perturbed fluid velocity and perturbed fluid pressure at  $x = L/2$  when  $c_o = 10$  m/s: (a) axial displacement,  $u$ ; (b) perturbed fluid velocity,  $c_d$ ; (c) perturbed fluid pressure,  $p_d$ .

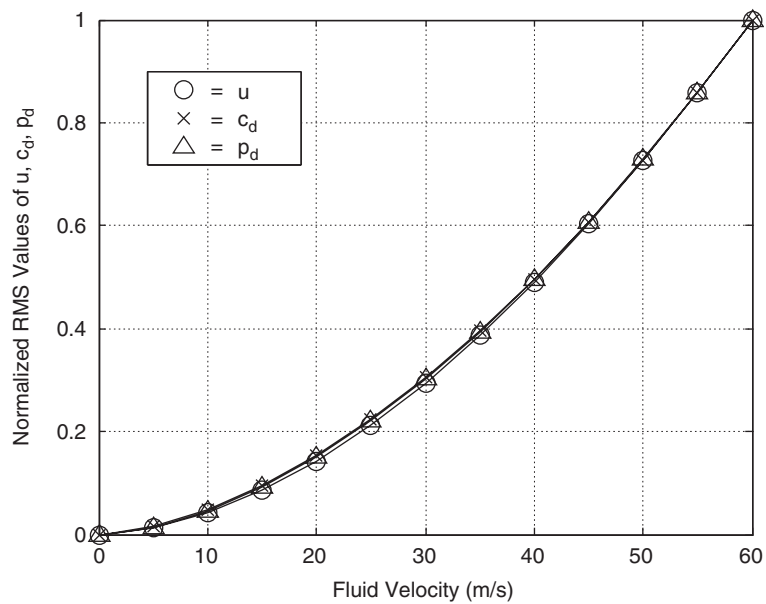


Fig. 9. Normalized root-mean-square (r.m.s.) values of the axial displacement ( $u$ ), perturbed fluid velocity ( $c_d$ ), and perturbed fluid pressure ( $p_d$ ) at  $x = L/2$  versus the fluid velocity  $c_o$ .

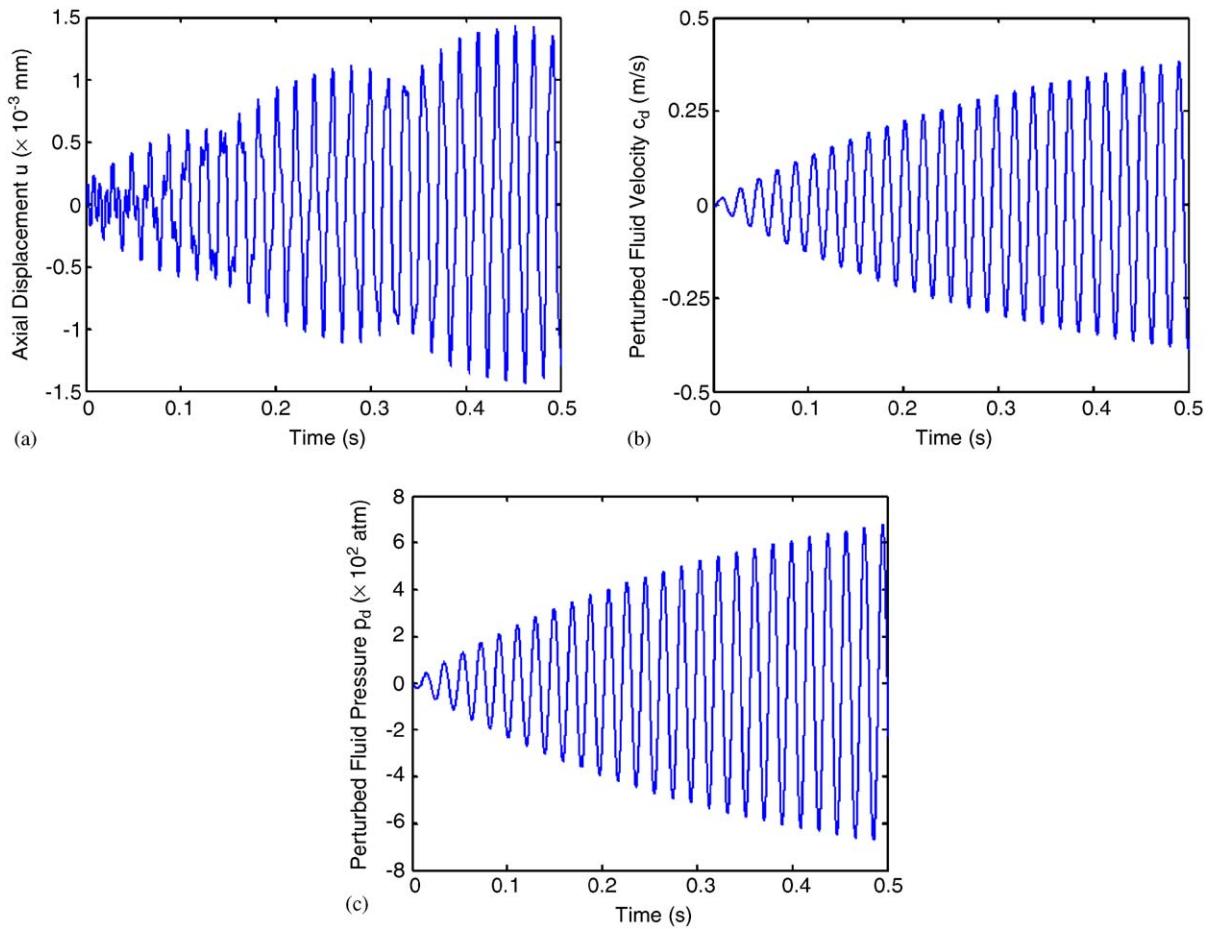


Fig. 10. The axial displacement and the perturbed fluid velocity and pressure at  $x = L/2$  when  $c_o = 10(1 + 0.001 \sin 102\pi t)$  m/s at the inlet of the pipeline.

mode at about  $c_o = 28.65$  m/s (i.e., divergence velocity,  $c_D$ ), and the flutter instability may occur in the coupled mode of the first and second bending modes at about  $c_o = 57.33$  m/s (i.e., flutter velocity,  $c_F$ ). This type of coupled-mode flutter can also be observed in some aeroelasticity problems (Dowell, 1995). Fig. 6 shows the time histories of the transverse displacement at four different fluid velocities, including the divergence and flutter velocities, and Fig. 7 shows the corresponding frequency response functions, i.e., receptances. For Figs. 6 and 7, the same point load as applied for Fig. 4 is applied to excite the pipeline and all dynamic responses are measured at  $x = L/5$ . As expected, the dynamic response indeed diverges at the divergence velocity  $c_D$ , and it shows a flutter behavior at the flutter velocity  $c_F$ . The small ripples appearing in Fig. 6(c) are due to inevitable computational errors.

The axial displacement is coupled with the perturbed fluid velocity. Eq. (16) shows that the axial displacement can be excited by the steady-state flow through the friction term  $mf c_o^2/2D$ , without need to apply an external excitation load. Therefore, both the axial displacement and the perturbed fluid velocity will generate the perturbed fluid pressure through the last equation of Eq. (16).

Fig. 8 shows the axial displacement  $u$ , the perturbed fluid velocity  $c_d$ , and the perturbed fluid pressure  $p_d$ , all measured at  $x = L/2$  when  $c_o = 10$  m/s. The root-mean-square (r.m.s.) values of  $u$ ,  $c_d$ , and  $p_d$  are shown in Fig. 9 as a function of fluid speed  $c_o$ . The r.m.s. values are computed from the corresponding time responses for 1.5 s. Fig. 9 shows that all r.m.s. values of  $u$ ,  $c_d$ , and  $p_d$  increase exponentially, in the quite similar pattern, as the fluid speed  $c_o$  increases.

When the inlet fluid velocity is controlled by  $c_o = 10(1 + 0.001 \sin 104\pi t)$  m/s, the axial displacement, the perturbed fluid velocity and the perturbed fluid pressure are shown in Fig. 10. Fig. 10 shows that all responses tend to rapidly

increase with time. This is because the excitation frequency of the inlet fluid velocity (i.e., 52 Hz) is chosen to be almost identical to the natural frequency of the first fluid mode at  $c_o = 10$  m/s (see Table 1) so that the resonance phenomenon occurs. Since the rapid increase of axial displacement and internal fluid pressure may result in serious structural failures, one may need to pay more attention whenever the inlet fluid has an excitation frequency very close to a natural frequency of the internal fluid.

### 5. Conclusions

In this study, a spectral element model is developed for the straight pipelines containing internal unsteady flow. First, a set of nonlinear, coupled pipe-dynamics equations is derived, in which the axial and transverse displacements of the pipeline and the fluid velocity and pressure of the internal flow are all considered as independent variables. Next, the coupled pipe-dynamics equations are linearized about the steady-state fluid pressure and velocity to derive a linear pipe-dynamics model, as the first approximation. The spectral element model is then formulated for the linear pipe-dynamics model by using the frequency-dependent shape functions exactly obtained from the linear pipe-dynamics equations. The high accuracy of the present spectral element model is numerically verified in due course by comparing the eigenfrequencies and dynamic responses obtained by the present SEM with those obtained by the conventional FEM and exact theory. Lastly, the spectral element analysis is conducted to investigate the stability and dynamic characteristics of an example pipeline conveying internal unsteady fluid.

### Appendix A

The finite element model used in this paper is formulated by using the displacement fields and fluid fields within a finite element of length  $l$  defined by

$$\begin{aligned} w(x, t) &= [N_w(x)]\{\mathbf{d}_w(t)\}, \\ u(x, t) &= [N_u(x)]\{\mathbf{d}_u(t)\}, \\ c_d(x, t) &= [N_c(x)]\{\mathbf{d}_c(t)\}, \end{aligned} \tag{A.1}$$

where  $\{\mathbf{d}_w(t)\}$ ,  $\{\mathbf{d}_u(t)\}$  and  $\{\mathbf{d}_c(t)\}$  are the vectors defined by

$$\begin{aligned} \{\mathbf{d}_w(t)\} &= \{w_1(t), \theta_1(t), w_2(t), \theta_2(t)\}^T, \\ \{\mathbf{d}_u(t)\} &= \{u_1(t), u_2(t)\}^T, \\ \{\mathbf{d}_c(t)\} &= \{c_1(t), c_2(t)\}^T \end{aligned} \tag{A.2}$$

and  $[N_w(x)]$ ,  $[N_u(x)]$  and  $[N_c(x)]$  are the shape function matrices defined by

$$\begin{aligned} [N_w(x)] &= [N_{w1}(x) \ N_{w2}(x) \ N_{w3}(x) \ N_{w4}(x)], \\ [N_u(x)] &= [N_{r1}(x) \ N_{r2}(x)], \\ [N_c(x)] &= [N_{r1}(x) \ N_{r2}(x)], \end{aligned} \tag{A.3}$$

where

$$\begin{aligned} N_{w1}(x) &= 1 - 3x^2/l^2 + 2x^3/l^3, \quad N_{w2}(x) = x - 2x^2/l + x^3/l^2, \\ N_{w3}(x) &= 3x^2/l^2 - 2x^3/l^3, \quad N_{w4}(x) = -x^2/l + x^3/l^2, \\ N_{r1}(x) &= 1 - x/l, \quad N_{r2}(x) = x/l. \end{aligned} \tag{A.4}$$

By following the conventional finite element formulation procedure (Reddy, 1993), the finite element equation is derived in the matrix form as

$$[M]\{\ddot{\mathbf{d}}\} + [C]\{\dot{\mathbf{d}}\} + [K]\{\mathbf{d}\} = \{\mathbf{f}\}, \tag{A.5}$$

where  $\{\mathbf{d}\}$  and  $\{\mathbf{f}\}$  are the nodal dofs vector and the nodal forces vector, respectively, defined by

$$\{\mathbf{d}(t)\} = \begin{Bmatrix} \mathbf{d}_w(t) \\ \mathbf{d}_u(t) \\ \mathbf{d}_c(t) \end{Bmatrix} = \begin{Bmatrix} w_1(t) \\ \theta_1(t) \\ w_2(t) \\ \theta_2(t) \\ u_1(t) \\ u_2(t) \\ c_1(t) \\ c_2(t) \end{Bmatrix}, \quad \{\mathbf{f}\} = \begin{Bmatrix} V_1(t) \\ M_1(t) \\ V_2(t) \\ M_2(t) \\ T_1(t) \\ T_2(t) \\ -\dot{p}_{d1}/d_1 \\ \dot{p}_{d2}/d_1 \end{Bmatrix} + \begin{Bmatrix} 0 \\ 0 \\ 0 \\ 0 \\ \int_0^l b_5[\mathbf{N}_u]^T dx \\ \phantom{\int_0^l b_5[\mathbf{N}_u]^T dx} \\ \phantom{\int_0^l b_5[\mathbf{N}_u]^T dx} \\ \phantom{\int_0^l b_5[\mathbf{N}_u]^T dx} \end{Bmatrix}_{4 \times 1}. \quad (\text{A.6})$$

and  $[\mathbf{M}]$ ,  $[\mathbf{C}]$  and  $[\mathbf{K}]$  are finite element matrices given by

$$[\mathbf{M}] = \begin{bmatrix} M_{ww} & \mathbf{0} & \mathbf{0} \\ \mathbf{0} & M_{uu} & \mathbf{0} \\ \mathbf{0} & M_{cu} & M_{cc} \end{bmatrix}, \quad (\text{A.7})$$

$$[\mathbf{C}] = \begin{bmatrix} C_{ww} & \mathbf{0} & \mathbf{0} \\ \mathbf{0} & \mathbf{0} & \mathbf{0} \\ C_{cw} & C_{cu} & C_{cc} \end{bmatrix},$$

$$[\mathbf{K}] = \begin{bmatrix} K_{ww} & \mathbf{0} & \mathbf{0} \\ K_{uw} & K_{uu} & K_{uc} \\ \mathbf{0} & \mathbf{0} & K_{cc} \end{bmatrix},$$

where

$$[M_{ww}] = m \int_0^l [\mathbf{N}_w]^T [\mathbf{N}_w] dx = ml \begin{bmatrix} \frac{13}{35} & \frac{11l}{210} & \frac{9}{70} & -\frac{13l}{420} \\ \frac{11l}{210} & \frac{l^2}{105} & \frac{13l}{420} & -\frac{l^2}{140} \\ \frac{9}{70} & \frac{13l}{420} & \frac{13}{35} & -\frac{11l}{210} \\ -\frac{13l}{420} & -\frac{l^2}{140} & -\frac{11l}{210} & \frac{l^2}{105} \end{bmatrix},$$

$$[M_{uu}] = m_p \int_0^l [\mathbf{N}_u]^T [\mathbf{N}_u] dx = \frac{m_p l}{6} \begin{bmatrix} 2 & 1 \\ 1 & 2 \end{bmatrix},$$

$$[M_{cu}] = \frac{c_o}{a^2} \int_0^l [\mathbf{N}'_c]^T [\mathbf{N}'_u] dx = \frac{c_o}{a^2 l} \begin{bmatrix} 1 & -1 \\ -1 & 1 \end{bmatrix},$$

$$[M_{cc}] = \frac{1}{a^2} \int_0^l [\mathbf{N}_c]^T [\mathbf{N}_c] dx = \frac{l}{6a^2} \begin{bmatrix} 2 & 1 \\ 1 & 2 \end{bmatrix},$$

$$[C_{ww}] = 2m_w c_o \int_0^l [\mathbf{N}_w]^T [\mathbf{N}'_w] dx = \frac{m_w c_o}{30} \begin{bmatrix} -30 & 6l & 30 & -6l \\ -6l & 0 & 6l & -l^2 \\ -30 & -6l & 30 & 6l \\ 6l & l^2 & -6l & 0 \end{bmatrix}, \quad (\text{A.8})$$

$$[C_{cw}] = \frac{g_Y}{a^2} \int_0^l [\mathbf{N}_c]^T [\mathbf{N}'_w] dx = \frac{g_Y}{12a^2} \begin{bmatrix} -6 & l & 6 & -l \\ -6 & -l & 6 & l \end{bmatrix},$$

$$[C_{cu}] = -2v \int_0^l [\mathbf{N}'_c]^T [\mathbf{N}'_u] dx = \frac{2v}{l} \begin{bmatrix} -1 & 1 \\ 1 & -1 \end{bmatrix},$$

$$[C_{cc}] = \frac{c_o}{a^2} \left[ \int_0^l [N_c]^T [N'_c] dx + \frac{f}{D} \int_0^l [N_c]^T [N_c] dx \right] = \frac{c_o}{a^2} \left( \frac{1}{2} \begin{bmatrix} -1 & 1 \\ -1 & 1 \end{bmatrix} + \frac{fl}{6D} \begin{bmatrix} 2 & 1 \\ 1 & 2 \end{bmatrix} \right),$$

$$[K_{ww}] = \int_0^l \{ EI_p [N''_w]^T [N''_w] + (p_o A + m_w c_o^2) [N_w]^T [N''_w] + T_o [N'_w]^T [N'_w] \} dx$$

$$= \frac{2EI_p}{l^3} \begin{bmatrix} 6 & 3l & -6 & 3l \\ 3l & 2l^2 & -3l & l^2 \\ -6 & -3l & 6 & -3l \\ 3l & l^2 & -3l & 2l^2 \end{bmatrix} + \frac{(p_o A + m_w c_o^2)}{30l} \begin{bmatrix} -36 & -33l & 36 & -3l \\ -3l & -4l^2 & 3l & l^2 \\ 36 & 3l & -36 & 33l \\ -3l & l^2 & 3l & -4l^2 \end{bmatrix}$$

$$+ \frac{T_o}{30l} \begin{bmatrix} 36 & 3l & -36 & 3l \\ 3l & 4l^2 & -3l & -l^2 \\ -36 & -3l & 36 & -3l \\ 3l & -l^2 & -3l & 4l^2 \end{bmatrix},$$

$$[K_{uw}] = -m_w g_Y \int_0^l [N_u]^T [N'_w] dx = \frac{m_w g_Y}{12} \begin{bmatrix} 6 & -l & -6 & l \\ 6 & l & -6 & -l \end{bmatrix},$$

$$[K_{uu}] = (EA_p + T_o) \int_0^l [N'_u]^T [N'_u] dx = \frac{(EA_p + T_o)}{l} \begin{bmatrix} 1 & -1 \\ -1 & 1 \end{bmatrix},$$

$$[K_{uc}] = -m_w \frac{fc_o}{D} \int_0^l [N_u]^T [N_c] dx = -m_w \frac{fc_o l}{6D} \begin{bmatrix} 2 & 1 \\ 1 & 2 \end{bmatrix},$$

$$[K_{cc}] = \int_0^l [N'_c]^T [N'_c] dx = \frac{1}{l} \begin{bmatrix} 1 & -1 \\ -1 & 1 \end{bmatrix}.$$

**References**

Ashley, H., Haviland, G., 1950. Bending vibrations of a pipeline containing flowing fluid. *Journal of Applied Mechanics* 72, 229–232.

Banerjee, J.R., 1997. Dynamic stiffness formulation for structural elements: a general approach. *Computers and Structures* 63, 101–103.

Blevins, R.D., 1979. *Formulas for Natural Frequency and Mode Shape*. Van Nostrand Reinhold Company, New York.

Chen, S.S., 1971. Dynamic stability of tube conveying fluid. *ASCE Journal of the Engineering Mechanics Division* 97, 1469–1485.

Dowell, E.H., 1995. *A Modern Course in Aeroelasticity*. Kluwer Academic Publishers, Dordrecht, The Netherlands.

Doyle, J.F., 1997. *Wave Propagation in Structures: Spectral Analysis Using Fast Discrete Fourier Transforms*, second ed. Springer, New York.

Gorman, D.G., Reese, J.M., Zhang, Y.L., 2000. Vibration of a flexible pipe conveying viscous pulsating fluid flow. *Journal of Sound and Vibration* 230, 379–392.

Hansen, A.G., 1967. *Fluid Mechanics*. Wiley, New York.

Hill, J.L., Davis, C.G., 1974. The effect of inertial forces on the hydroelastic vibration and stability of planar curved tubes. *Journal of Applied Mechanics*, 355–359.

Housner, G.W., 1952. Bending vibrations of a pipeline containing flowing fluid. *Journal of Applied Mechanics* 19, 205–209.

Jensen, J.S., 1997. Fluid transport due to nonlinear fluid–structure interaction. *Journal of Fluids and Structures* 11, 327–344.

Koo, G.H., Park, Y.S., 1998. Vibration reduction by using periodic supports in a piping systems. *Journal of Sound and Vibration* 210, 53–68.

Lee, S.I., Chung, J., 2002. New non-linear modeling for vibration analysis of a straight pipe conveying fluid. *Journal of Sound and Vibration* 254, 313–325.

Lee, U., 2004. *Spectral Element Method in Structural Dynamics*. Inha University Press, Inha University, Incheon, Korea.

Lee, U., Kim, J., 1999. Dynamics of branched pipeline systems conveying internal unsteady flow. *Journal of Vibration and Acoustics* 121, 114–122.

Lee, U., Oh, H., 2003. The spectral element model for pipelines conveying internal steady flow. *Engineering Structures* 25, 1045–1055.

- Lee, U., Pak, C.H., Hong, S.C., 1995. The dynamics of a piping system with internal unsteady flow. *Journal of Sound and Vibration* 180, 297–311.
- Lee, U., Kim, J., Leung, A.Y.T., 2000. The spectral element method in structural dynamics. *The Shock and Vibration Digest* 32, 451–465.
- Lesmez, M.W., Wiggert, D.C., Hatfield, F.J., 1990. Modal analysis of vibrations in liquid-filled piping systems. *ASME Journal of Fluids Engineering* 109, 311–318.
- Lin, Y.H., Tsai, Y.K., 1997. Nonlinear vibrations of Timoshenko pipes conveying fluid. *International Journal of Solids and Structures* 34, 2945–2956.
- Nemat-Nasser, S., Prasad, S.N., Hermann, G., 1966. Destabilizing effect of velocity-dependent forces in nonconservative continuous systems. *AIAA Journal* 4, 1276–1280.
- Öz, H.R., 2001. Non-linear vibrations and stability analysis of tensioned pipes conveying fluid with variable velocity. *International Journal of Non-linear Mechanics* 36, 1031–1039.
- Païdoussis, M.P., 1998. *Fluid–Structure Interactions: Slender Structures and Axial Flow*, vol. 1. Academic Press, London.
- Païdoussis, M.P., 2003. *Fluid–structure Interactions: Slender Structures and Axial Flow*, vol. 2. Elsevier Academic Press, London.
- Païdoussis, M.P., Li, G.X., 1993. Pipes conveying fluid: a model dynamical problem. *Journal of Fluids and Structures* 7, 137–204.
- Païdoussis, M.P., Luu, T.R., Laithier, B.E., 1986. Dynamics of finite-length tubular beams conveying fluid. *Journal of Sound and Vibration* 106, 311–331.
- Reddy, J.N., 1993. *An Introduction to the Finite Element Method*. McGraw-Hill, New York.
- Semler, C., Li, G.X., Païdoussis, M.P., 1994. The non-linear equations of motion of pipes conveying fluid. *Journal of Sound and Vibration* 169, 577–599.
- Stein, R.A., Tobriner, W.M., 1970. Vibration of pipes containing flowing fluids. *Journal of Applied Mechanics*, 906–916.
- Zhang, Y.L., Gorman, D.G., Reese, J.M., 1999. Analysis of the vibration of pipes conveying fluid. *Journal of Mechanical Engineering Science* 213, 849–860.
- Zhang, Y.L., Reese, J.M., Gorman, D.G., Madhok, R., 2002. The vibration of an artery-like tube conveying pulsatile fluid flow. *Proceedings of the Institution of Mechanical Engineers, Part H, Journal of Engineering in Medicine* 216, 1–11.
- Zhang, Y.L., Reese, J.M., Gorman, D.G., 2003. An experimental study of the effects of pulsatile fluid flow on an elastic tube subjected to external vibration. *Journal of Sound and Vibration* 266, 355–367.